On the all-India rainfall index and sub-India rainfall heterogeneity

Spencer A. Hill[1], **Adam H. Sobel**[1,2], **Michela Biasutti**[1], **and Mark A. Cane**[1]

[1]Lamont-Doherty Earth Observatory, Columbia University, Palisades, New York
[2]Department of Applied Physics and Applied Mathematics and Lamont-Doherty Earth Observatory, Columbia University, New York, New York

Key Points:

- We examine Indian summer monsoon rainfall interannual variability and teleconnections 1901-2020
- All-India Rainfall Index (AIRI) closely tracks spatial and temporal extent of wet anomalies
- ENSO teleconnection projects onto AIRI but Indian Ocean Dipole onto a known tripole pattern

Corresponding author: Spencer A. Hill, `shill@ldeo.columbia.edu`

Abstract

We revisit longstanding controversies regarding summer-mean relationships among the all-India rainfall index (AIRI), sub-India rainfall, El Niño-Southern Oscillation (ENSO), and the Indian Ocean Dipole (IOD) using 120-year sea surface temperature and high-resolution rainfall datasets. AIRI closely tracks with the spatial extent of wet anomalies and with the average across gridpoints in rainy day count. The leading rainfall variability mode is a monopole associated primarily with rainy day count and ENSO. The second mode is a tripole with same-signed loadings in the high-rainfall Western Ghats and Central Monsoon Zone regions and opposite-signed loadings in Southeastern India between. The IOD projects onto this tripole and, as such, is weakly correlated with AIRI. However, when the linear influence of ENSO is removed, the IOD rainfall regressions become quasi-homogeneously more positive, making the ENSO-residual IOD and AIRI timeseries significantly correlated.

Plain Language Summary

The Indian summer monsoon generates copious rainfall each June through September, but more in some years than others, and more in some Indian sub-regions than others. We use observational datasets spanning 1901-2020 to reconcile past disagreements about these fluctuations. There has long been concern that the rainfall rate averaged over the whole summer and whole of India—the All-India Rainfall Index—doesn't necessarily track with the spatial extent of wet or dry anomalies within India which is more relevant for many societal purposes, but we show that the two measures vary closely with one another. There has been disagreement about how the all-India average relates to rainfall in fixed sub-regions of India, and we show using high-resolution rainfall data that the issue stems in part from the use of coarse datasets in the past. Finally, we reconcile disagreements about whether or not the Indian Ocean Dipole (IOD) teleconnection influences all-India rainfall by showing that, when the El Niño-Southern Oscillation signal that influences both the IOD and the monsoon rains is removed, the IOD significantly influences the all-India average and with a distinct sub-India spatial pattern.

1 Introduction

Rainfall averaged across India and over June-July-August-September (JJAS)—the All-India Rainfall index (AIRI)—is a widely used, physically intuitive, and societally relevant (Mooley et al., 1981; Parthasarathy et al., 1988; Gadgil, 1995; Gadgil & Gadgil, 2006) bulk indicator of the summer monsoon. But its use is controversial, largely owing to summer monsoon rainfall's pronounced sub-India and sub-seasonal heterogeneity. Summer rainfall is high within a broad band of northern-central India, higher still within a narrow band in the southwest between the Arabian Sea and the Western Ghats mountains, and much lower in southeastern India between these two bands. And throughout the subcontinent JJAS rainfall variability is much higher on daily than interannual timescales (Krishnamurthy & Shukla, 2000). In this study we address three long-running controversies regarding AIRI's interpretation in light of this spatiotemporal variability, attempting to synthesize and reconcile past arguments made with differing and often short and/or coarse datasets by using state-of-the-art, 120-year datasets of Indian rainfall at high resolution and of sea surface temperature (SST).

First is the relationship between AIRI and the overall spatiotemporal extent of wetting or drying across India. Spatially, in most summers there are parts of India that experience drought and others excess rainfall, and for e.g. rain-fed agriculture quite plausibly the spatial extent of drought relative to local rainfall normals is more relevant than the average rainfall anomaly in mm day^{-1} across India (Parthasarathy et al., 1993). This has motivated attempts to define bulk indices in terms of the fraction of the Indian surface area experiencing rainfall anomalies exceeding specified thresholds (Mooley et al.,

1981; Parthasarathy et al., 1987). Temporally, a recent series of studies (Moron et al., 2012, 2017; Robertson et al., 2019) employ a useful decomposition of JJAS-mean rainfall at any given point into the product of the frequency of rainy days and the mean rainfall intensity on rainy days, arguing that rainy day frequency tends to be more spatially coherent across India and thus potentially predictable. We will make use of this decomposition to construct and compare alternative indices to AIRI.

Second is the relationship between AIRI and rainfall anomalies over geographically fixed sub-India regions. The literature on dividing India into so-called "coherent" or "homogeneous" sub-regions—i.e. over which rainfall interannual variability tends to be similar—dates to the 19th century (see Shukla (1987); Parthasarathy et al. (1993); Gadgil et al. (1993) and references therein). Subseasonally, it is well established that the predominant variability mode—the so-called active-break cycle—comprises a tripole: in active periods, rainfall is enhanced over the Western Ghats (henceforth WG) and Central Monsoon Zone (henceforth CMZ) bands but suppressed over southeastern India (henceforth SEI) (Rajeevan et al., 2010). And because the CMZ and WG anomalies are larger than the SEI anomalies in absolute terms, AIRI is enhanced (the same results hold with signs reversed for break periods). Interannually, the predominant mode is instead a quasi-uniform wetting or drying across the subcontinent that strongly projects onto AIRI (Shukla, 1987; Krishnamurthy & Shukla, 2000, 2007, 2008; Straus & Krishnamurthy, 2007; Mishra et al., 2012; Moron et al., 2012, 2017). A second seasonal-mean variability mode has been identified (Krishnamurthy & Shukla, 2008) but characterized by Mishra et al. (2012) as a north-south dipole rather than the CMZ-SEI-WG tripole, with generally same-signed anomalies across peninsular India including both the WG and SEI, and opposite-signed conditions to the north including the CMZ. This would seem consistent with the argument put forth separately that seasonal-mean rainfall anomalies in the CMZ and WG are weakly correlated, and that therefore AIRI effectively amounts to the superposition of two quasi-independent processes (Vecchi & Harrison, 2004). We will revisit both arguments using a $0.25^\circ \times 0.25^\circ$ rainfall dataset that better resolves the sharp rainfall gradient between the WG and SEI regions.

Third is the relationship between both AIRI and sub-India rainfall anomalies to teleconnection modes emanating from the tropical Pacific and Indian Oceans. The link between the Indian summer monsoon and the El Niño-Southern Oscillation (ENSO) is well established, with drought more likely in El Niño summers and excess rain in La Niña summers (Pant & Parthasarathy, 1981; Rasmusson & Carpenter, 1983), both at the all-India scale and most individual points (excluding the far northeast for reasons described below). Nevertheless, ENSO indices have always left the majority of AIRI variance unexplained (Surendran et al., 2015), even before a weakening of the ENSO-AIRI lag-zero correlation in recent decades compared to the mid 20th century (Kumar et al., 1999; Ashok et al., 2019). The Indian Ocean Dipole (IOD)—the zonally oriented oscillatory mode spanning the equatorial Indian ocean (Saji et al., 1999; Webster et al., 1999)—has been argued to modulate ENSO's influence on AIRI (Ashok et al., 2001, 2004), with the IOD-AIRI correlation relatively high in decades when the ENSO-AIRI correlation is relatively low and vice versa. While it has been argued that the IOD is in fact largely controlled by ENSO (Krishnamurthy & Kirtman, 2003; Stuecker et al., 2017), Ashok and Saji (2007) argue that the IOD spatial imprint on Indian summer monsoon rainfall is much more heterogeneous, concentrated roughly over the CMZ region. Meanwhile, other studies focused on the atmospheric counterpart to the IOD, the Equatorial Indian Ocean Oscillation, have argued that the correlation between the IOD and AIRI is effectively zero (Gadgil et al., 2004; Ihara et al., 2007; Surendran et al., 2015). We will attempt to reconcile these arguments by examining the spatial imprint of the IOD and ENSO on rainfall amount, rainy-day frequency, and mean rainfall intensity (c.f. Moron et al. (2017)) and by isolating the IOD and ENSO signals from one another (c.f. (Ashok & Saji, 2007)).

After describing the datasets and methods used (Section 2), we argue the following (Section 3): AIRI is an excellent indicator of the spatial extent of wet anomalies across the subcontinent; the second leading mode of interannual variability is the familiar CMZ-SEI-WG tripole; rainfall anomalies within the CMZ and WG regions are well correlated; ENSO strongly imprints on the leading monopole pattern and thus AIRI while the IOD imprints on the tripole pattern and thus weakly on AIRI; and when the ENSO signal is linearly removed the IOD influence becomes more positive at most points such that the ENSO-residual IOD and AIRI timeseries are significantly correlated. We then conclude with summary and discussion (Section 4).

2 Methods

For rainfall, we use the Indian Meteorological Department (IMD) daily, gridded $0.25\times0.25^\circ$ dataset spanning 1901-2020, which is derived from a dense but time-varying network of rain gauges across India comprising 6,955 total and on average ∼2,600 operational each year (Pai et al., 2014). Daily values from 1 June to 30 September each year are averaged to form a JJAS seasonal mean. No further temporal filtering is employed. We have compared the IMD dataset with the TRMM 3B42v7 (Huffman et al., 2007) daily dataset over the period 1998-2014. On individual days the differences between the datasets can be substantial (not shown), but the JJAS-mean AIRI timeseries computed with the two datasets are highly correlated ($r = 0.94$). We distinguish rainy days from non-rainy days using a 1 mm day^{-1} threshold, with results very similar if 0 mm day^{-1} is used instead (not shown).

As common in studies of the summer monsoon (Parthasarathy et al., 1988; Krishnamurthy & Shukla, 2000; Vecchi & Harrison, 2004), we exclude points in far north and northeast India, in our case by applying the "monsoonal India" mask of Gadgil et al. (2019). In far northern India the terrain makes rain gauges less reliable and representative, and the vicinity to the Himalayas and extratropical influences make interannual rainfall variability not clearly related to the summer monsoon circulation. For Northeast India there appear to be spurious data points in a cluster of grid cells on the border of Bangladesh, with the JJAS mean and variance jumping in 1971 to implausible values over the remainder of the record (not shown). Nonetheless, the mean JJAS rainfall timeseries with or without the monsoon mask are highly correlated ($r = 0.95$); henceforth we refer to the monsoonal-India average as AIRI.

We use standard SST-based indices of ENSO and the IOD—the NINO3.4 and Dipole Mode Index (DMI; Saji et al. (1999)) respectively—computed with monthly SSTs spanning years 1901-2020 from the NOAA Extended Reconstruction SST (Huang et al., 2015) dataset (ERSST) version 5. NINO3.4 is defined as the average SST anomaly spanning 120-170°W, 5°S-5°N, and DMI is defined as the difference between the SST anomalies averaged over a western equatorial Indian Ocean box (50-70°E, 10°S-0°) and over an eastern equatorial Indian Ocean box (90-110°E, 10°S-10°N). Anomalies are defined as the deviation at each gridpoint from the local climatology over 1901-2020 for that month, with June through September anomalies then averaged to yield JJAS values for each index. The correlation with AIRI is virtually unchanged if NINO3.4 is replaced by the NINO3 index (both $r = -0.53$) and moderately weakened for NINO4 ($r = -0.40$), and rainfall regression and correlation patterns also look very similar for each of the three NINO indexes (not shown).

The AIRI, gridpoint-local rainfall, ENSO, and DMI JJAS-mean, 120-yr timeseries are each detrended by subtracting the linear trend over 1901-2020 from simple least squares regression. Trends over 1901-2020 are weak in the IMD rainfall dataset at the vast majority of gridpoints, and all major results we present are insensitive to the detrending (not shown). For all detrended JJAS timeseries analyzed the interannual autocorrelations are sufficiently weak and the distributions are sufficiently normal (not shown) that

a simple t-test yields a reasonable measure of statistical significance; in particular, using a conservative estimate of 100 degrees of freedom yields significance at the 5% level for correlations with $|r| > 0.195$. Though note that for spatially gridded data this point-by-point approach may overstate significance due to spatial autocorrelations (Wilks, 2016).

3 Results

3.1 AIRI relationship to spatiotemporal extent of rainfall anomalies

Fig. 1(a) shows the climatological JJAS rainfall and its interannual standard deviation for each gridpoint. The standard deviation largely scales with the local climatological mean, and both are heterogeneous—high within CMZ, highest within WG, and much lower in SEI. Fig. 1(b) shows the fraction of annual-mean rainfall that occurs in JJAS as well as surface elevation contours. The JJAS rainfall fraction exceeds 95% in parts of the far western CMZ, exceeds 80% over most of the WG and CMZ, and does not exceed 50% in most of SEI, where in the far southeast the rainy season occurs during the northeast monsoon in boreal autumn (Ramesh et al., 2021). The elevation contours highlight how southwesterly low-level summer monsoon flow largely perpendicular to the Western Ghats mountain range axis results in a concentrated rainfall band on the windward side and a much broader and drier regime on the leeward side over the Deccan Plateau (Francis & Gadgil, 2006; Flynn et al., 2017; Hunt et al., 2021). Fig. 1(c) shows the climatological number of rainy days in JJAS and the mean rainfall rate on those rainy dates. Rain falls nearly every summer day within most of WG, most days within most of the CMZ, and less frequently within most of SEI. Mean rainfall intensity is highest within WG directly along the coast, with a sharp gradient moving inland up the mountain slope, with smoother spatial variations elsewhere.

Given this heterogeneity, in principle AIRI need not be a useful indicator of the spatial extent of wet or dry anomalies: an average across regions with high variance and regions with low variance will depend primarily on the former and weakly on the latter. We have therefore constructed six alternative all-India measures of JJAS rainfall variability: first, the average standardized rainfall anomaly (i.e. the raw anomaly divided by the standard deviation, rather than just the raw anomaly as for AIRI); second, the number of gridpoints in which the local JJAS rainfall anomaly is positive; third, the average across all gridpoints of the number of rainy days; fourth, the average across all gridpoints of the rainfall rate on rainy days; fifth, the mean rainfall anomaly restricting to those gridpoints for which the rainfall anomaly is positive; and sixth, the mean rainfall anomaly restricting to those gridpoints for which the rainfall anomaly is negative. The first, third, and fourth variants were introduced by Moron et al. (2017).

Fig. 2 provides a cross-correlation matrix of AIRI and these six alternative measures (along with numerous additional fields below the first horizontal line to be discussed below). Among AIRI and the first three variants—which characterize the spatial or temporal extent of wet anomalies—all correlation coefficients exceed 0.9. Among AIRI and the last three variants, which characterize the intensity of wet or dry anomalies, no correlation coefficient exceeds 0.77. Thus, AIRI depends more on the spatiotemporal extent of rainfall across India and JJAS than on the severity of rainfall anomalies when and where they occur. This agrees with Moron et al. (2017), who also note that this contrasts with interannual variability at the gridpoint scale: for most gridpoints of monsoonal India the JJAS rainfall amount depends more on the intensity of rain events than the number of rainy days.

We therefore conclude that AIRI is an excellent indicator of the overall spatial extent of wet or dry anomalies, as well as of the average anomaly in rainy day occurrence across India. Insofar as the latter two measures are more directly relevant to agricultural and thus economic outcomes, this helps explain the high correlations found by previous

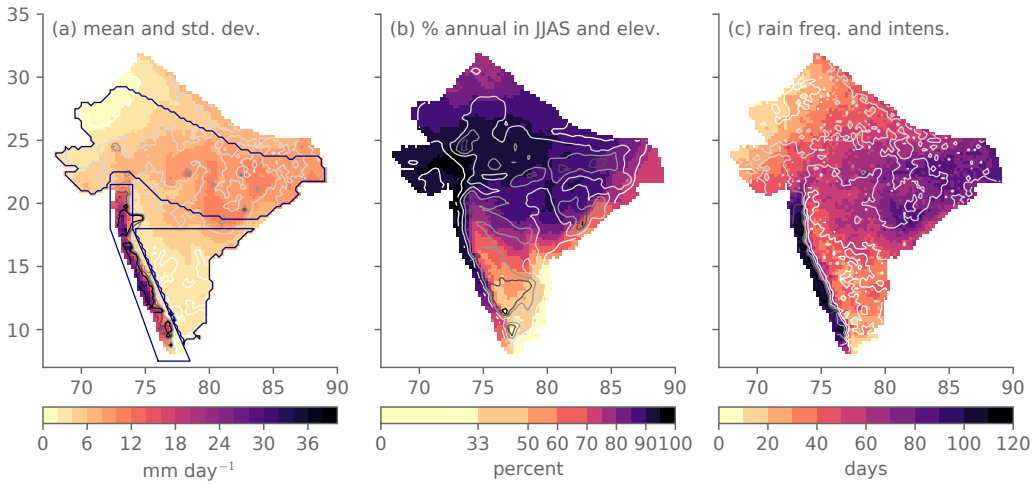

Figure 1. (a) Climatological JJAS rainfall mean in color shading and standard deviation in contours in the IMD 0.25×0.25° gridded dataset, 1901-2020. Standard deviation contours from white to black are 1, 2, 3, 4, and 5 mm day^{-1} (maximum standard deviation is 14.2 mm day^{-1}). (b) Climatological fraction of annual-mean rainfall that occurs during JJAS in color shading and surface elevation in contours. Elevation contours from white to black are 100, 300, 500, 700, and 900 m (maximum elevation is 1028 m). (c) Climatological mean number of rainy days in JJAS in color shading and mean rainfall intensity on rainy days in contours. Mean rainfall intensity contours from white to black are 10, 15, 20, 25, and 30 mm day^{-1} (maximum mean rainfall intensity is 44.8 mm day^{-1}. Blue outlines in panel a and in subsequent figures show the borders of the three sub-India regions we analyze in detail, namely the Central Monsoon Zone (CMZ) in the north, Western Ghats (WG) in the southwest, and Southeastern India (SEI) in the southeast.

studies of AIRI itself with agricultural yields and gross domestic product on interannual timescales (Mooley et al., 1981; Parthasarathy et al., 1988; Gadgil, 1995; Gadgil & Gadgil, 2006).

3.2 Rainfall relationships among fixed sub-India regions

We have repeated the empirical orthogonal function (EOF) analyses of Moron et al. (2017) for JJAS standardized anomalies in each of rainfall mean, rainy day frequency, and mean rainfall intensity; our calculations include more recent years and, more importantly, the second EOF for rainfall amount (c.f. Mishra et al. (2012)) in addition to each first EOF. Fig. 3 shows these EOFs, and Fig. 2 reports correlation coefficients among the corresponding principal component (PC) timeseries as well as AIRI. The first EOF of rainfall amount accounts for 18.2% of the total variance and consists of same-signed loadings at the vast majority of gridpoints (Krishnamurthy & Shukla, 2000). This resembles the first EOF of rainy day frequency, which explains 32.4% of the rainy day frequency variance and exhibits an even more homogeneous pattern, though sharing the two local minima located east of the WG mountains axis and in the far east. The PC timeseries corresponding to these amount and frequency first EOFs are each highly correlated with AIRI ($r = 0.96$ and 0.93, respectively).

Both the first EOF of mean rainfall intensity (7.2% of variance) and the second EOF of rain amount (9.3% of variance) comprise a CMZ-SEI-WG tripole pattern. The corresponding PCs are highly correlated with one another ($r = 0.85$) but weakly with AIRI.

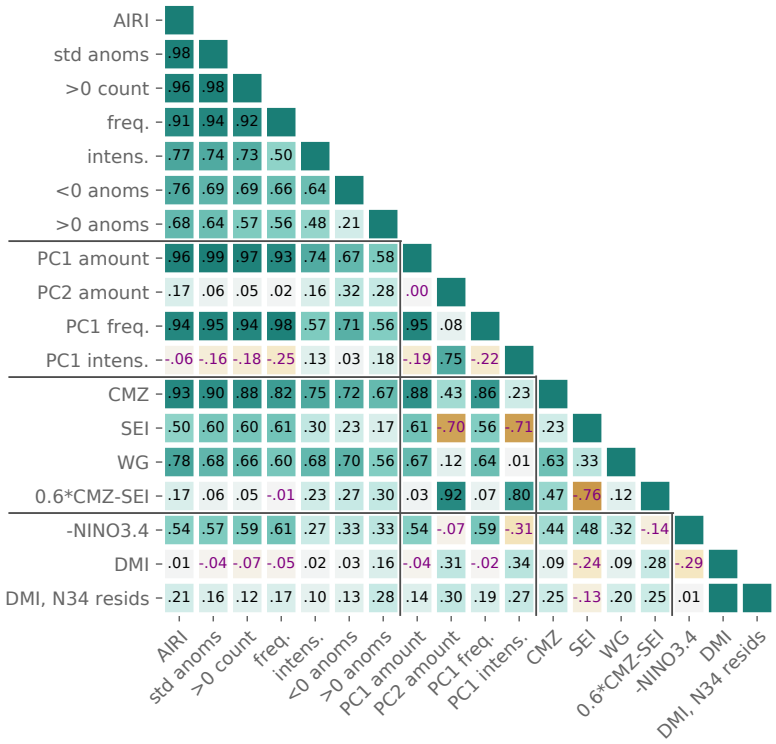

Figure 2. Cross-correlation matrix showing the correlation coefficients (unitless) among AIRI, six variants thereof as defined in the text, four PC timeseries as described in the text, regional rainfall averages over each of the CMZ, SEI, and WG regions and a linear combination of CMZ and SEI as described in the text, and the NINO3.4 (with sign reversed) and DMI timeseries, all for JJAS and over the 1901-2020 period. For the final row only, labeled "DMI, N34 resids", both the DMI timeseries and all target timeseries are the residuals after linearly removing the NINO3.4 signal. Horizontal and vertical lines separate the timeseries into categories: AIRI and variants thereof, PC timeseries, sub-region averages, and teleconnection indices, respectively from top to bottom and left to right.

Unlike for rainfall amount and rainy day frequency, the first EOF for mean rainfall intensity is not well separated in variance explained from the remaining EOFs (the second EOF, not shown, accounts for 5.5%). But its physical relevance is supported by the correspondence of its pattern to the rainfall EOF2 and to the IOD teleconnection results we will present below.

We compute averages over each of the CMZ, WG, and SEI sub-regions using border definitions as follows (shown as blue contours in Figs. 1a, 3, and 4). The CMZ boundaries follow Gadgil et al. (2019). We define the non-coastal borders of WG to align with the sharp rainfall gradient separating the coastal and inland peninsular regimes, and define SEI to be all gridpoints east thereof and south of 18°N. Pointwise correlation maps (not shown) indicate that rainfall in points within the CMZ tends to vary positively both with other CMZ points and with points within WG, but weakly or negatively with those in SEI; the region-mean JJAS rainfall correlations are $r = 0.23$, 0.63, and 0.33 respectively for CMZ-SEI, CMZ-WG, and SEI-WG.

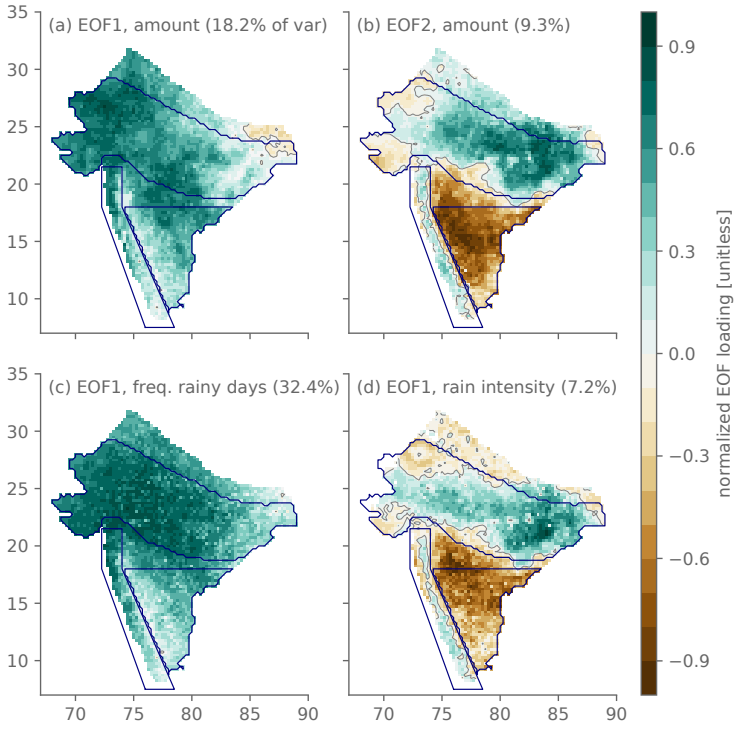

Figure 3. (a) First and (b) second EOF of JJAS rainfall amount, and first EOF of (c) rainy day frequency, and (d) rainfall intensity, each with the percentage of variance explained by that EOF printed in the top-left. EOFs were computed from standardized anomalies in each case. In each panel, values are normalized by that EOF's maximal value, and solid gray contours signify that EOF's zero contour.

Using the CMZ, SEI, and WG regional averages, we have constructed one, two, and three-region linear regression models for AIRI and for the tripole mode, the latter defined by the rain amount PC2 (results are similar if the intensity PC1 is used instead; not shown). For AIRI, at $r = 0.93$ the CMZ alone explains most of the variance as shown by Gadgil et al. (2019), leaving little additional skill to be gained by including either of the other regions. For the tripole mode, by contrast, the highest-magnitude single-region correlation is with SEI at $r = -0.70$. The CMZ-SEI two-region model, whose relative weights are 0.6 and -1 respectively and whose timeseries is included in Fig. 2 along with the three individual region averages, yields $r = 0.92$ with the tripole mode. This is effectively unchanged by including the WG as well.

Thus, despite WG being home to the highest JJAS-mean rainfall variances throughout monsoonal India, it adds little predictive power to CMZ and SEI for these bulk measures, due to it being well correlated with CMZ ($r = 0.63$). This is considerably higher than two similar-but-different regions ($r \approx 0.2$) reported by Vecchi and Harrison (2004). That study's WG region (borders overlain in Fig. 4d), based on coarse 2.5×2.5° gridded CMAP rainfall data, spans into peninsular India and thus includes points for which rainfall anomalies are anti-correlated with those along the coast. The correspondence between WG and CMZ rainfall anomalies has also been established through cluster analysis of seasonal-mean rainfall anomalies by Moron et al. (2017) using 0.25°×0.25° data.

We conclude that the sharp rainfall gradients in the southwest—which have dictated the border definitions of subdivisions of the Indian Meteorological Department sta-

tion network since the 19th century (Kelkar & Sreejith, 2020)—are insufficiently resolved in gridded datasets with resolutions of 1° or more. With higher resolution the second interannual variability mode after the quasi-uniform first mode is a CMZ-SEI-WG tripole (a semblance of the tripole is visible in Fig. 1 of Mishra et al. (2012) based on 0.5×0.5° data, but it is described in their text as a north-south dipole). As such, the CMZ and WG mean rainfall anomalies cannot be considered quasi-independent (Vecchi & Harrison, 2004).

3.3 ENSO and IOD teleconnections

Fig. 2 includes the -1×NINO3.4 and DMI timeseries, the sign of NINO3.4 flipped so that positive values correspond to positive AIRI anomalies. The correlation between -1×NINO3.4 and AIRI is $r = 0.54$, between $-1\times$NINO3.4 and DMI is $r = -0.29$, and between DMI and AIRI nearly zero, $r = 0.01$, all broadly consistent with past studies. Using partial correlation analysis to remove the linear NINO3.4 signal from both rainfall and the DMI timeseries, the resulting DMI and AIRI residual timeseries become significantly positively correlated, $r = 0.21$. In El Niño years removing the NINO3.4 signal increases AIRI and makes the DMI more positive, and similarly with signs reversed for La Niña years, and this is why the AIRI-DMI correlation becomes more positive. Conversely, removing the DMI signal hardly affects the ENSO-AIRI relationship ($r = 0.56$), and mechanisms through which ENSO influences the IOD are well documented (Stuecker et al., 2017). We therefore now analyze the spatial imprints of ENSO and the IOD on the Indian summer monsoon via the rainfall frequency-intensity decomposition, in the case of the IOD focusing on the NINO3.4 residuals (c.f. last row of Fig. 2).

Fig. 4(a-c) shows the correlation of each of JJAS rainfall amount, rainy day frequency, and mean rainfall intensity with $-1\times$NINO3.4. For rainfall amount, the correlation is positive at most gridpoints, most positive within SEI and the central portion of CMZ, and least positive (including some slightly negative values) in the far east of the CMZ and along the Western Ghats mountain axis. The rainy day frequency correlation is more homogeneously positive and with higher magnitudes in most areas, especially along the Arabian Sea coast within WG and the central and western CMZ. The mean rainfall intensity correlation is noisier and has generally weaker magnitudes, with a considerable fraction of gridpoints below the approximate statistical significance threshold of $|r| \gtrsim 0.2$ described in Section 2. It takes the reverse sign over an appreciable fraction of gridpoints including much of the CMZ, and of the three sub-regions it is most consistently positive over SEI. These three spatial patterns are broadly comparable to the corresponding first EOFs for JJAS rainfall amount (mostly same-signed), frequency (more homogeneous than amount), and intensity (heterogeneous with a CMZ-SEI-WG tripole, the modest statistical significance notwithstanding).

Fig. 4(d-f) show the correlations between the NINO3.4-residual timeseries of DMI and JJAS rainfall amount, rainy day frequency, and mean rainfall intensity at each gridpoint. For amount and frequency, the predominant signal is a WG-SEI-CMZ tripole, with positive IOD events moderately correlated with excess rain over most of the WG and CMZ and deficient rain over SEI. Unlike for NINO3.4, the patterns in rainfall amount, rainy day frequency, and mean rainfall intensity are all grossly similar—to first order, all three are CMZ-SEI-WG tripoles, just with more positive values overall for rainy day frequency and more negative values overall for mean rainfall intensity. Though the values over most gridpoints for all three are insignificant on statistical grounds, the correspondence of all three patterns to the physically well-grounded tripole mode argues against them being purely artifacts. Moreover, the tripole structure helps explain why the full, non-residual DMI timeseries correlation with AIRI is very small ($r = 0.01$) but significantly larger for the tripole indicators ($r = 0.31$ for amount PC2, $r = 0.34$ for intensity PC1).

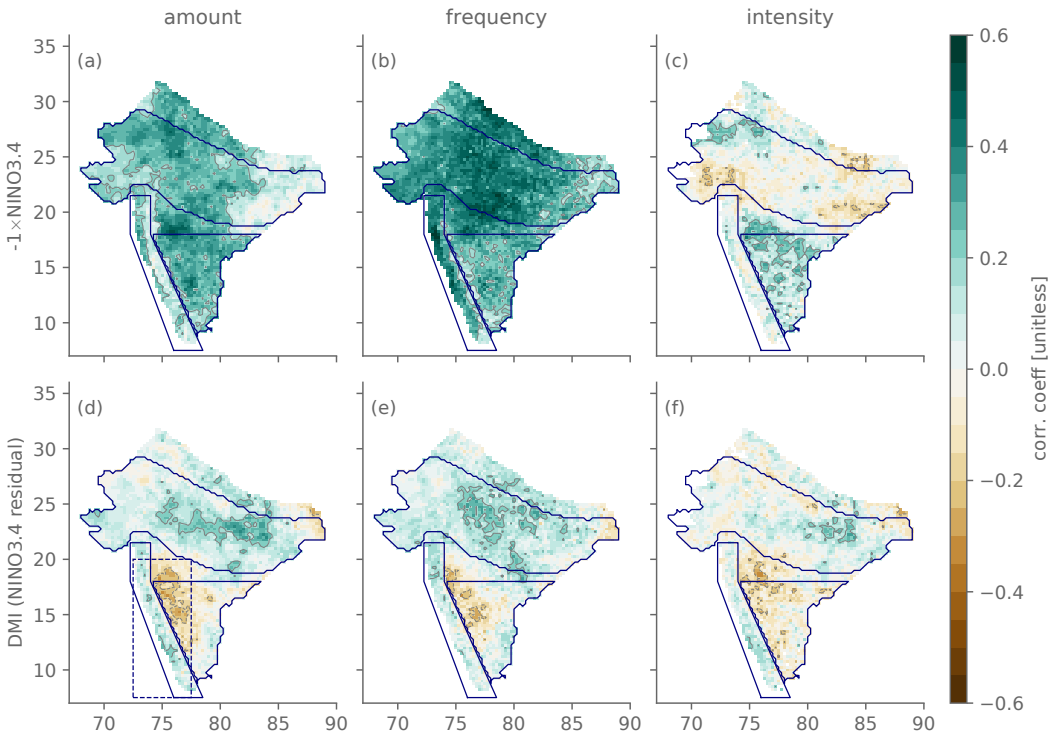

Figure 4. Top row, correlation coefficient between JJAS -1×NINO3.4 and gridpoint local (a) rainfall amount, (b) frequency of rainy days, and (c) mean rainfall intensity. Overlain in thin gray are the -0.2 and +0.2 contours, which give a reasonable estimate of statistical significance as described in Section 2. Bottom row, panels d-f repeat a-c but with the NINO3.4 index replaced by the DMI, and with the linear influence of NINO3.4 on both rainfall and DMI removed via a partial correlation calculation. Dashed box in (d) shows the WG region border used by Vecchi and Harrison (2004).

We conclude that, while it is the case that DMI is weakly correlated with AIRI, the IOD imprints a familiar spatial pattern, the WG-SEI-CMZ tripole. Moreover, when the quasi-uniform drying influence of ENSO is linearly removed, the DMI correlations become quasi-uniformly more positive, and as such the component of AIRI interannual variance not associated with ENSO is signficantly related to the IOD.

4 Conclusions

We use observational datasets of SST and high-resolution gridded rainfall spanning 1901-2020 to revisit three controversies in the literature involving relationships among the June-July-August-September (JJAS) seasonal averages of the All-India Rainfall Index (AIRI), the sub-India spatial distribution of rainfall variability, ENSO, and the IOD. The first is the extent to which AIRI is representative of the spatiotemporal extent of rainfall anomalies. Despite past concerns raised to the contrary, AIRI is found to be an excellent indicator of the spatial extent of wet anomalies across monsoonal India, and additionally of the average anomalous number of rainy days. It is less closely related to the severity of rainfall anomalies when and where they occur.

The second is how AIRI variability relates to rainfall in fixed sub-India regions, and the third is how variability in AIRI and the subregions relate to ENSO and the IOD. We

confirm prior analyses of the leading variability mode via EOF analysis: it is a quasi-homogeneous wetting or drying that results primarily from an even more homogeneous and stronger signal in rainy day frequency, and it is strongly influenced by ENSO. The second mode is a tripole with same-signed loadings in the high-rainfall Central Monsoon Zone and Western Ghats regions and opposite loadings in Southeastern India between. This mode is associated more with rainfall intensity than with rainy day frequency and is effectively unrelated to ENSO. The IOD imprints appreciably on the tripole mode and, with respect to the residual fields with the ENSO signal removed, imprints significantly on AIRI as well.

Acknowledgments

All authors acknowledge support from the Monsoon Mission Project under India's Ministry of Earth Sciences. S.A.H. acknowledges funding from the Columbia University Earth Institute Postdoctoral Fellowship. We thank Sulochana Gadgil for many valuable discussions and comments. We thank P. Mukhopadhyay for helpful comments. IMD rainfall data used is available at `https://www.imdpune.gov.in/Clim_Pred_LRF_New/Grided_Data_Download.html`. ERSST data is available at `https://www.ncei.noaa.gov/pub/data/cmb/ersst/v5/netcdf/`

References

Ashok, K., Feba, F., & Tejavath, C. T. (2019, July). The Indian summer monsoon rainfall and ENSO. *Mausam*, *70*(10), 443–452.

Ashok, K., Guan, Z., Saji, N. H., & Yamagata, T. (2004, August). Individual and Combined Influences of ENSO and the Indian Ocean Dipole on the Indian Summer Monsoon. *J. Climate*, *17*(16), 3141–3155. doi: 10.1175/1520-0442(2004)017⟨3141:IACIOE⟩2.0.CO;2

Ashok, K., Guan, Z., & Yamagata, T. (2001). Impact of the Indian Ocean dipole on the relationship between the Indian monsoon rainfall and ENSO. *Geophysical Research Letters*, *28*(23), 4499–4502. doi: 10.1029/2001GL013294

Ashok, K., & Saji, N. H. (2007, August). On the impacts of ENSO and Indian Ocean dipole events on sub-regional Indian summer monsoon rainfall. *Nat Hazards*, *42*(2), 273–285. doi: 10.1007/s11069-006-9091-0

Flynn, W. J., Nesbitt, S. W., Anders, A. M., & Garg, P. (2017). Mesoscale precipitation characteristics near the Western Ghats during the Indian Summer Monsoon as simulated by a high-resolution regional model. *Quarterly Journal of the Royal Meteorological Society*, *143*(709), 3070–3084. doi: 10.1002/qj.3163

Francis, P. A., & Gadgil, S. (2006, November). Intense rainfall events over the west coast of India. *Meteorol. Atmos. Phys.*, *94*(1), 27–42. doi: 10.1007/s00703-005-0167-2

Gadgil, S. (1995). Climate change and agriculture – An Indian perspective. *Current Science*, *69*(8), 649–659.

Gadgil, S., & Gadgil, S. (2006). The Indian Monsoon, GDP and Agriculture. *Economic and Political Weekly*, *41*(47), 4887–4895.

Gadgil, S., Rajendran, K., & Pai, D. S. (2019, July). A new rain-based index for the Indian summer monsoon rainfall. *Mausam*, *70*(3), 485–500.

Gadgil, S., Vinayachandran, P. N., Francis, P. A., & Gadgil, S. (2004, June). Extremes of the Indian summer monsoon rainfall, ENSO and equatorial Indian Ocean oscillation. *Geophysical Research Letters*, *31*(12), L12213. doi: 10.1029/2004GL019733

Gadgil, S., Yadumani, & Joshi, N. V. (1993). Coherent rainfall zones of the Indian region. *International Journal of Climatology*, *13*(5), 547–566. doi: 10.1002/joc.3370130506

Huang, B., Banzon, V. F., Freeman, E., Lawrimore, J., Liu, W., Peterson, T. C., ...

Zhang, H.-M. (2015, February). Extended Reconstructed Sea Surface Temperature Version 4 (ERSST.v4). Part I: Upgrades and Intercomparisons. *J. Climate*, *28*(3), 911–930. doi: 10.1175/JCLI-D-14-00006.1

Huffman, G. J., Bolvin, D. T., Nelkin, E. J., Wolff, D. B., Adler, R. F., Gu, G., ... Stocker, E. F. (2007, February). The TRMM Multisatellite Precipitation Analysis (TMPA): Quasi-Global, Multiyear, Combined-Sensor Precipitation Estimates at Fine Scales. *J. Hydrometeor*, *8*(1), 38–55. doi: 10.1175/JHM560.1

Hunt, K. M. R., Turner, A. G., Stein, T. H. M., Fletcher, J. K., & Schiemann, R. K. H. (2021). Modes of coastal precipitation over southwest India and their relationship with intraseasonal variability. *Quarterly Journal of the Royal Meteorological Society*, *147*(734), 181–201. doi: 10.1002/qj.3913

Ihara, C., Kushnir, Y., Cane, M. A., & Peña, V. H. D. L. (2007). Indian summer monsoon rainfall and its link with ENSO and Indian Ocean climate indices. *International Journal of Climatology*, *27*(2), 179–187. doi: 10.1002/joc.1394

Kelkar, R. R., & Sreejith, O. P. (2020, October). Meteorological sub-divisions of India and their geopolitical evolution from 1875 to 2020. *Mausam*, *71*(4), 571–584.

Krishnamurthy, V., & Kirtman, B. P. (2003). Variability of the Indian Ocean: Relation to monsoon and ENSO. *Quarterly Journal of the Royal Meteorological Society*, *129*(590), 1623–1646. doi: 10.1256/qj.01.166

Krishnamurthy, V., & Shukla, J. (2000, December). Intraseasonal and Interannual Variability of Rainfall over India. *J. Climate*, *13*(24), 4366–4377. doi: 10.1175/1520-0442(2000)013⟨0001:IAIVOR⟩2.0.CO;2

Krishnamurthy, V., & Shukla, J. (2007, January). Intraseasonal and Seasonally Persisting Patterns of Indian Monsoon Rainfall. *J. Climate*, *20*(1), 3–20. doi: 10.1175/JCLI3981.1

Krishnamurthy, V., & Shukla, J. (2008, March). Seasonal persistence and propagation of intraseasonal patterns over the Indian monsoon region. *Clim Dyn*, *30*(4), 353–369. doi: 10.1007/s00382-007-0300-7

Kumar, K. K., Rajagopalan, B., & Cane, M. A. (1999, June). On the Weakening Relationship Between the Indian Monsoon and ENSO. *Science*, *284*(5423), 2156–2159. doi: 10.1126/science.284.5423.2156

Mishra, V., Smoliak, B. V., Lettenmaier, D. P., & Wallace, J. M. (2012, May). A prominent pattern of year-to-year variability in Indian Summer Monsoon Rainfall. *PNAS*, *109*(19), 7213–7217. doi: 10.1073/pnas.1119150109

Mooley, D. A., Parthasarathy, B., Sontakke, N. A., & Munot, A. A. (1981). Annual rain-water over India, its variability and impact on the economy. *Journal of Climatology*, *1*(2), 167–186. doi: 10.1002/joc.3370010206

Moron, V., Robertson, A. W., & Ghil, M. (2012, June). Impact of the modulated annual cycle and intraseasonal oscillation on daily-to-interannual rainfall variability across monsoonal India. *Clim Dyn*, *38*(11), 2409–2435. doi: 10.1007/s00382-011-1253-4

Moron, V., Robertson, A. W., & Pai, D. S. (2017, November). On the spatial coherence of sub-seasonal to seasonal Indian rainfall anomalies. *Clim Dyn*, *49*(9), 3403–3423. doi: 10.1007/s00382-017-3520-5

Pai, D. S., Sridhar, L., Rajeevan, M., Sreejith, O. P., Satbhai, N. S., & Mukhopadhyay, B. (2014). Development of a new high spatial resolution ($0.25^\circ \times 0.25^\circ$) long period (1901-2010) daily gridded rainfall data set over India and its comparison with existing data sets over the region. *Mausam*, *65*(1), 18.

Pant, G. B., & Parthasarathy, S. B. (1981, September). Some aspects of an association between the southern oscillation and indian summer monsoon. *Arch. Met. Geoph. Biocl., Ser. B*, *29*(3), 245–252. doi: 10.1007/BF02263246

Parthasarathy, B., Kumar, K. R., & Munot, A. A. (1993, March). Homogeneous Indian Monsoon rainfall: Variability and prediction. *Proc. Indian Acad. Sci. (Earth Planet Sci.)*, *102*(1), 121–155. doi: 10.1007/BF02839187

Parthasarathy, B., Munot, A. A., & Kothawale, D. R. (1988, March). Regression model for estimation of indian foodgrain production from summer monsoon rainfall. *Agricultural and Forest Meteorology*, *42*(2), 167–182. doi: 10.1016/0168-1923(88)90075-5

Parthasarathy, B., Sontakke, N. A., Monot, A. A., & Kothawale, D. R. (1987). Droughts/floods in the summer monsoon season over different meteorological subdivisions of India for the period 1871–1984. *Journal of Climatology*, *7*(1), 57–70. doi: 10.1002/joc.3370070106

Rajeevan, M., Gadgil, S., & Bhate, J. (2010, June). Active and break spells of the Indian summer monsoon. *J Earth Syst Sci*, *119*(3), 229–247. doi: 10.1007/s12040-010-0019-4

Ramesh, N., Nicolas, Q., & Boos, W. R. (2021, July). The Globally Coherent Pattern of Autumn Monsoon Precipitation. *Journal of Climate*, *34*(14), 5687–5705. doi: 10.1175/JCLI-D-20-0740.1

Rasmusson, E. M., & Carpenter, T. H. (1983, March). The Relationship Between Eastern Equatorial Pacific Sea Surface Temperatures and Rainfall over India and Sri Lanka. *Mon. Wea. Rev.*, *111*(3), 517–528. doi: 10.1175/1520-0493(1983)111⟨0517:TRBEEP⟩2.0.CO;2

Robertson, A. W., Moron, V., Vigaud, N., Acharya, N., Greene, A. M., & Pai, D. S. (2019, April). Multi-scale variability and predictability of Indian summer monsoon rainfall. *Mausam*, *70*(2), 277–292.

Saji, N. H., Goswami, B. N., Vinayachandran, P. N., & Yamagata, T. (1999, September). A dipole mode in the tropical Indian Ocean. *Nature*, *401*(6751), 360–363. doi: 10.1038/43854

Shukla, J. (1987). Interannual Variability of Monsoons. In *Monsoons* (pp. 399–464).

Straus, D. M., & Krishnamurthy, V. (2007). The Preferred Structure of the Interannual Indian Monsoon Variability. In M. Sharan & S. Raman (Eds.), *Atmospheric and Oceanic: Mesoscale Processes* (pp. 1717–1732). Basel: Birkhäuser. doi: 10.1007/978-3-7643-8493-7_15

Stuecker, M. F., Timmermann, A., Jin, F.-F., Chikamoto, Y., Zhang, W., Wittenberg, A. T., ... Zhao, S. (2017). Revisiting ENSO/Indian Ocean Dipole phase relationships. *Geophysical Research Letters*, *44*(5), 2481–2492. doi: 10.1002/2016GL072308

Surendran, S., Gadgil, S., Francis, P. A., & Rajeevan, M. (2015, September). Prediction of Indian rainfall during the summer monsoon season on the basis of links with equatorial Pacific and Indian Ocean climate indices. *Environ. Res. Lett.*, *10*(9), 094004. doi: 10.1088/1748-9326/10/9/094004

Vecchi, G. A., & Harrison, D. E. (2004). Interannual Indian Rainfall Variability and Indian Ocean Sea Surface Temperature Anomalies. In *Earth's Climate: The Ocean-Atmosphere Interaction* (pp. 247–259). American Geophysical Union (AGU). doi: 10.1029/147GM14

Webster, P. J., Moore, A. M., Loschnigg, J. P., & Leben, R. R. (1999, September). Coupled ocean–atmosphere dynamics in the Indian Ocean during 1997–98. *Nature*, *401*(6751), 356–360. doi: 10.1038/43848

Wilks, D. S. (2016, March). "The Stippling Shows Statistically Significant Grid Points": How Research Results are Routinely Overstated and Overinterpreted, and What to Do about It. *Bull. Amer. Meteor. Soc.*, *97*(12), 2263–2273. doi: 10.1175/BAMS-D-15-00267.1